View Online / Journal Homepage / Table of Contents for this issue
Dynamic Article Links

CrystEngComm

Cite this: *CrystEngComm*, 2012, **14**, 4596–4600

www.rsc.org/crystengcomm

PAPER

Top down fabrication of organic nanocrystals by femtosecond laser induced transfer method

Hong-Hua Fang,[a] Jie Yang,[b] Ran Ding,[a] Jing Feng,*[a] Qi-Dai Chen[a] and Hong-Bo Sun*[ac]

Received 24th November 2011, Accepted 5th April 2012
DOI: 10.1039/c2ce06579g

We present the preparation of nanometer-size organic crystals using femtosecond laser induced forward transfer (Fs-LIFT) method. 1,4-Bis(4-methylstyryl)benzene (BSB-Me) nanocrystals are directly deposited on the substrate to form a nanocrystal film. Size and morphology as functions of applied laser fluence are investigated. We show that monodispersed organic nanoparticles with size varying from 40 nm to 300 nm could be obtained by careful adjustment of the experimental conditions. The produced nanoparticles exhibit well defined shapes, such as cube and tetrahedron with rather sharp edges. The as-prepared products have been characterized by means of X-ray diffraction, field-emission scanning electron microscopy, transmission electron microscopy (TEM), high-resolution TEM and selected area electron diffraction. The organic nanoparticles are demonstrated single crystalline, and FTIR spectra before and after the Fs-LIFT process shows that no significant chemical decomposition occurs during the process.

1. Introduction

The investigation of nanoparticles of low-molecular-weight functional compounds is currently a rapidly growing field due to their fundamental and technological importance and potential applications in the fields such as optoelectronics, nonlinear optics, and photonics.[1–12] Such nanoparticles of organic molecular materials very often represent an intermediate state, lying in between that of molecular solutions and bulk solid phases of the respective material.[13,14] This makes them deviate from the properties of the bulk and monodisperse molecules. It has been demonstrated that the optical properties can also be modulated by the particle size and shape.[15–22] The properties of organic nanocrystals, on the other hand, are fundamentally different from their inorganic counterparts (metals and inorganic semiconductors), due to weak intermolecular interaction forces of the van der Waals type.

To obtain nanoparticles, the reprecipitation method is a simple and convenient way, which is proposed by Nakanishi and co-workers.[23–25] In this method, a solution of the organic material dissolved in a solvent is added into an excess of a poor or non-solvent. This leads to supersaturation of the solution, and the organic material consequently precipitates, forming a dispersion of submicrometer-sized particles. However, it is difficult to precisely control the complicated nucleation process in the initial stages and the subsequent fast growth, and it is not applicable for organic materials that are only sparingly soluble in organic solvents (such as pentacene). Another common approach to nanoparticle preparation is based on pulsed-laser ablation of large, several-micrometer-sized, organic crystals suspended in a liquid.[26–28] These organic crystals absorb the laser light leading to a local increase in temperature and evaporation of a small amount of material from the crystal surface. Vaporized material is rapidly cooled by the surrounding liquid to form nanoparticles. The formation process and the optical properties of the nanoparticles are then strongly affected by the liquid environment.[29] Moreover, some of the organic compounds may interact with water or aqueous solution. These may lead the dispersed nanocrystals to be unstable in the liquid and affect or even change their properties, even if these processes are very slow.[30]

For this reason, we propose dry preparation of organic nanocrystals based on the femtosecond laser-induced forward transfer (Fs-LIFT) method.[31–34] In the Fs-LIFT, a pulsed laser beam is focused through a transparent support (quartz substrate) onto a thin film of the bulk crystal, the crystal then is fragmented, transferred and deposited onto a receptor. This allows the transferred materials deposited on the substrate to form a nanocrystal film with defined pattern. By careful adjustment of the experimental conditions, we show that monodispersed organic nanoparticles with well defined shapes could be obtained and it excluded the effects of liquid.

[a]*State Key Laboratory on Integrated Optoelectronics, College of Electronic Science and Engineering, Jilin University, 2699 Qianjin Street, Changchun 130012, China. E-mail: jingfeng@jlu.edu.cn; hbsun@jlu.edu.cn http://www.lasun-jlu.cn/index.php*
[b]*Guangdong Engineering Research Center for Semiconductor Lighting, School of Science, South China University of Technology, 381 Wushan Road, Tianhe District, Guangzhou, 510640, China*
[c]*College of Physics, Jilin University, 119 Jiefang Road, Changchun, 130023, China*

2. Experiments

A schematic diagram of the organic nanoparticles fabrication setup is depicted in Fig. 1. A regenerative amplifier (Spitfire, Spectra Physics) seeded with a mode-locked Ti:sapphire laser (Tsunami, Spectra Physics) was used, which emit laser pulses with 1 KHz repetition rate, 120 fs pulse duration at wavelength of 800 nm. The energy of laser pulse was controlled by neutral density filters. The laser beam was focused by a lens with a focal length of 600 mm on the crystal target surface with a spot of about 250 μm diameter. The fabrication process was under atmospheric pressure and at room temperature.

The materials used in our work were 1,4-bis(4-methylstyryl)benzene (BSB-Me) (Fig. 2), a typical optoelectronic functional material,[35,36] which was purchased from Tokyo Chemical Industry Co., Ltd. and was used without further treatment. The crystals, used as the "target", were prepared according to the method as described in the previous study.[35] The grown bulk crystals were transferred on to the transparent quartz wafers. Quartz or silicon substrates were used as the "receiver". The distance between the target and the receiver surfaces was variable from 60 μm to 10 mm. The target–receiver pair was fixed onto a computer-controlled x–y translation stage, allowing a maximum 25–25 mm movement.

The morphologies of as-prepared organic crystals were characterized by a field emission scanning electron microscope (JSM-7500F, JEOL) and high-resolution transmission electron microscope (HRTEM) (Tecnai F30). The Fourier transform infrared spectroscopy (FTIR) was recorded on a spectrometer (Thermo Scientific, Nicolet 6700) from 4000–400 cm^{-1}. UV-vis absorption and fluorescence measurements were recorded on a UV-3100 and a highly sensitive spectrometer (Avantes AvaSpec-2048), respectively. The fluorescence lifetime was recorded with a time-correlated single-photon counting (TCSPC) system under right-angle sample geometry. A 405 nm picosecond diode laser (Edinburgh Instruments EPL405, repetition rate 20 MHz) was used to excite the sample. The emission was detected by a photomultiplier tube (Hamamatsu H5783p) and a TCSPC board (Becker & Hickel SPC-130). The instrument response function is about 220 ps.

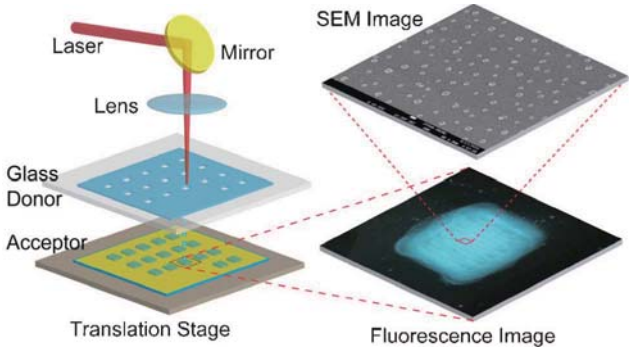

Fig. 1 Schematics of the femtosecond laser-induced forward transfer (Fs-LIFT) apparatus for the dry preparation of organic nanocrystals.

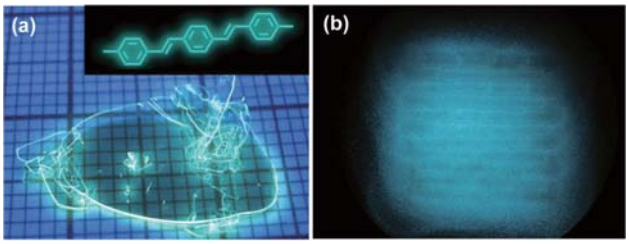

Fig. 2 (a) Optical photographs of single crystals of BSB-Me grown by physical vapor method under the UV light irradiation. Inset: the molecular structure of BSB-Me. (b) The production on the acceptor investigated by fluorescence microscope.

3. Results and discussion

The target materials used in the experiment are bulk organic crystals. Fig. 2 shows the image of the BSB-Me crystals under the excitation of UV light. The typical sizes for these materials are 1 × 1 cm in size with a thickness of several to tens of micrometers. The symmetry of crystal is orthorhombic with unit cell parameters a = 7.36 Å, b = 5.88 Å, c = 38.95 Å; $\alpha = 90^\circ$, $\beta = 90^\circ$, $\gamma = 90^\circ$. The crystals were adhered to the substrate and irradiated under the femtosecond laser beam. The laser spot moved point by point on the crystal's surface. After irradiation under the femtosecond laser, a film of material formed on the acceptor, as shown in Fig. 2b. This material was then characterized by scanning electron microscopy.

An amorphous-like film mixed with irregular micrometer size particles was produced when the laser fluence was high. Fig. 3 shows the products under femtosecond laser irradiation with relative high laser fluence. At laser fluence of 163 mJ $pulse^{-1}$ cm^{-2}, as shown in Fig. 3a, the products are amorphous-like, mixed with uneven micrometer size particles. As the laser fluence decreases (122 mJ $pulse^{-1}$ cm^{-2}), the abundance of particles decreases, and irregular products with micrometer size could be found, as shown in Fig. 3b. Further decreases of the laser fluence led the proportion of nano-scale particles to increase, while the number of micrometer size particles reduced greatly. Fig. 3c and 3d show the materials produced at fluence of 81 mJ $pulse^{-1}cm^{-2}$.

It is demonstrated that when the middle-level laser fluence was applied, uniform particles with nanoscale size could be obtained.

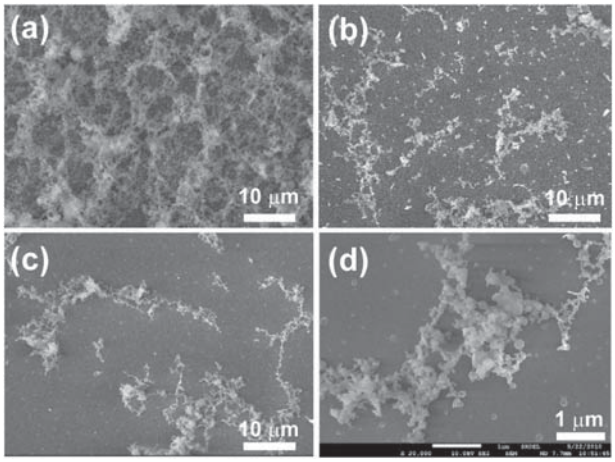

Fig. 3 SEM image of the materials produced by different laser fluences. (a) 163 mJ $pulse^{-1}$ cm^{-2}, (b) 122 mJ $pulse^{-1}$ cm^{-2}, (c) 81 mJ $pulse^{-1}$ cm^{-2}, (d) 30 mW, 81 mJ $pulse^{-1}$ cm^{-2}.

Fig. 4 shows the nanoparticles fabricated at middle-level laser fluence. The size of as-prepared BSB-Me nanoparticles is largely dependent on the laser fluence. To reveal the relationship between the particle size and the laser fluence, laser fluence was carefully adjusted, while other parameters, such as laser spot and irradiation time were kept constant. Fig. 4a shows the SEM image on the acceptor where the laser fluence is 20 mJ pulse^{-1} cm^{-2}. The prepared nanoparticles are fairly monodisperse. The corresponding histogram of the size distribution is shown in the right of Fig. 4(a). The particle size is about 40 nm with a narrow size distribution. The average size increases and the distribution broadens with an increase in the laser power. The histogram show that the average sizes are about 70 nm and 160 nm when the fluence is 30 mJ pulse^{-1} cm^{-2} and 50 mJ pulse^{-1} cm^{-2}, respectively. From the results, it can be concluded that smaller laser fluence is a benefit to the preparation of more monodisperse and smaller size nanoparticles.

The SEM studies show that the prepared nanocrystals present well defined shapes. Fig. 5b–f show the magnified SEM images of nanocrystals in Fig. 5a. As shown in Fig. 5b, a nanocuboid with rather sharp edges was produced. Most nanoparticles are cubic in geometry. It is very interesting that particles with other geometries could be found in addition to the cube, such as well-faceted tetrahedral-shaped nanocrystals, truncated cubes and truncated tetrahedra. The proportion of nanocrystals with these shapes is less than 10%. Surface energy and mechanical stability of each shape should be responsible for the geometry of the particles but we have not found any suggestive data to show a correlation between the shape and experimental conditions. The cell parameters show that the bulk crystal possesses an orthorhombic crystal system. This may be the possible reason that most of the obtained nanocrystals are cubic in geometry.

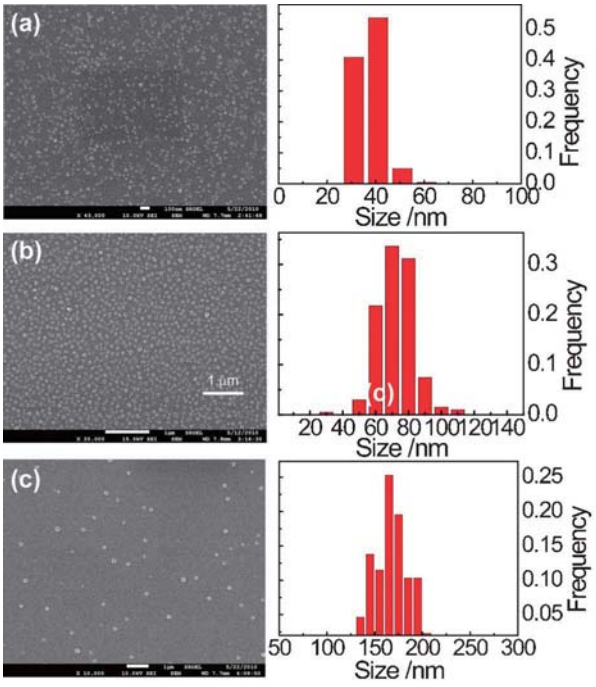

Fig. 4 SEM images and corresponding size distribution histograms (right) of the samples prepared with laser intensity of (a) 20 mJ pulse^{-1} cm^{-2} , (b) 30 mJ pulse^{-1} cm^{-2}, (c) 40 mJ pulse^{-1} cm^{-2}.

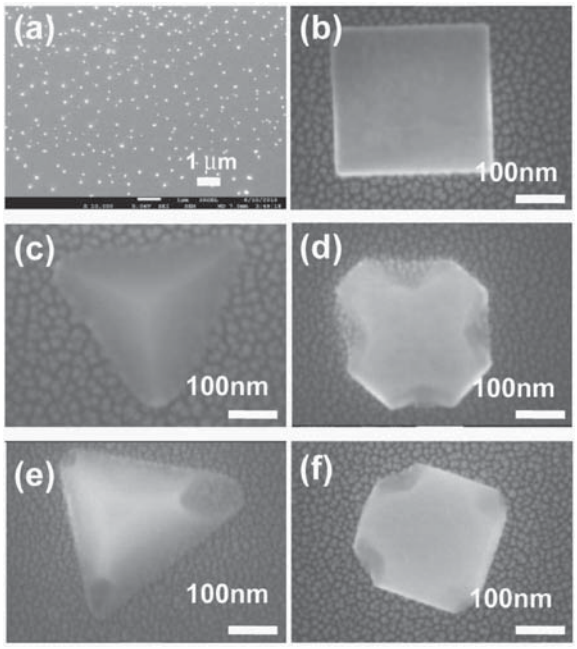

Fig. 5 (a) Products obtained under 60 mJ pulse^{-1} cm^{-2}. (b)–(f) Nanocrystals with different shapes produced.

The particles show great difference in contrast to the samples prepared by sublimation, where the nanoparticles are irregularly shaped. The nanoparticles were also prepared under the protection of argon gas, and showed no great difference. Further experiments are conducted to explore gas nature and pressure effect on the particles morphologies.

To investigate more detailed information of the nanocrystals, TEM and selected area electron diffraction (SAED) were used to characterize the configuration and crystalline structure of the nanocuboids. Fig. 6(a) shows the electron diffraction pattern obtained by directing the electron beam perpendicular to one of the square faces of a cube. The square symmetry of the spots

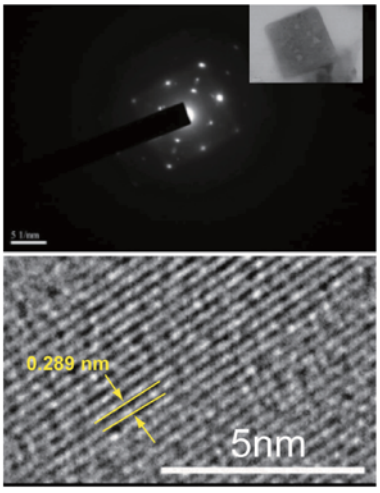

Fig. 6 (a) The SAED pattern of the nanocrystal in TEM image. (b) HRTEM image of the nanocrystal, the lattice fringe image can be observed.

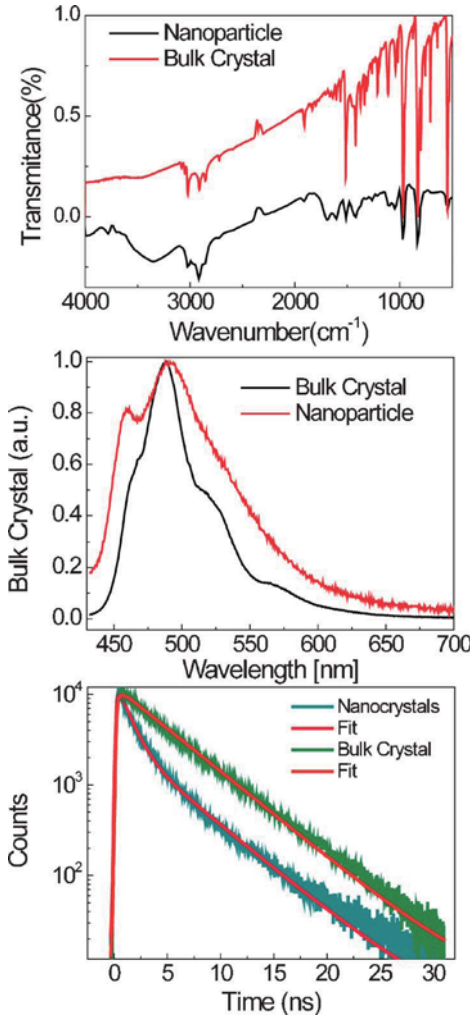

Fig. 7 (a) FT-IR spectra of BSB-Me nanocrystals and BSB-Me bulk crystals. (b) Fluorescence spectra of the BSB-Me nanocrystals and bulk crystals. (d) Time-resolved fluorescences of the BSB-Me nanocrystals and bulk crystals.

indicates that the organic nanocrystal is single-crystalline, and enclosed by {100} facets. Further evidence of the crystalline nature of the nanoparticles was obtained from the HRTEM studies (Fig. 6(b)). The well-defined lattice fringes (lattice fringe spacing is 0.289 nm) confirms the crystalline nature of the nanoparticles.[35]

FTIR of nanocrystals and bulk crystals were comparatively studied in Fig. 7(a). The homology in the FTIR spectra of the crystals and nanoparticles proved that the as-prepared nanocrystals have not undergone significant chemical decomposition during the Fs-LIFT process. Steady-state photoluminescence (PL) spectra of the BSB-Me nanocrystals were also measured at room temperature using the excitation wavelength of 405 nm. Fig. 7b shows the PL spectra of prepared nanocrystals. Compared with that of the bulk material, the PL peaks centered at 480 nm are the same as that of the bulk crystal, while the half-maximum (FWHM) of the PL was 92 nm and 54 nm for the nanocrystals and the bulk, respectively. A blue band at around 460 nm is more apparent in the nanocrystals. Self-absorption reduction in nanocrystals may be responsible, where the blue light is less absorbed. The structural defects may be another reason for the broadened spectrum. To assess the relative contributions of the radiative and nonradiative channels to nanocrystal PL decay, we compared PL lifetimes (detected at λ = 480 nm) for nanocrystals and bulk materials as shown in Fig. 7(c). The PL dynamics differ appreciably. Nearly mono-exponential PL decays attest to the bulk crystal, and their life time is about t = 4.6 ns. The data for the nanocrystals could be fitted with a double exponential decay (t_1 = 1.1 ns (0.78), t_2 = 4.6 ns (0.22)). This implies the formation of new energy levels, such as structural defects arising from the large surface-to-volume ratio of nanoparticles.

The morphology of the ablated region of bulk crystals have also been studied. Fig. 8 shows the SEM images of the results on the bulk crystals with 122 mJ pulse^{-1} cm^{-2}.

Nanostructures with well defined structures formed at the region on the ablated region, and no heat-affected zone was observed. Fig. 9(a)–(c) shows the morphology irradiated by the femtosecond laser pulses with intensity at 40 mJ pulse^{-1} for 10 pulses. Looking at the holes on the crystal surface it displays clear cracks and sharp edges. It is noted that it shows great difference in contrast to the inorganic materials such as metals and other inorganic semiconductors. These may arise from the different interactions of building blocks, where the organic crystals are held together by van der Waals forces, while covalent bonds bind the atoms in the inorganic semiconductors. The van der Waals forces are much weaker than that of covalent bonds, and make the organic crystal much more brittle. The analysis of the crystal structures demonstrates that the molecules are arranged layer by layer in the BSB-Me crystal. Each BSB-Me molecule connects with four adjacent molecules through these three aromatic CH–π hydrogen bonds. The molecules assemble themselves into rigid three-dimensional supramolecular interaction networks. In this network, the interactions within each layer are strong, while the interactions between layers are weak.[35] It could be deduced that the materials most likely break at these positions during the transient interaction between the intensive laser pulse and the crystals. Under the femtosecond laser interactions, the ultra-fast duration is shorter than the time of mechanical relaxation (expansion) of the absorbing volume, and

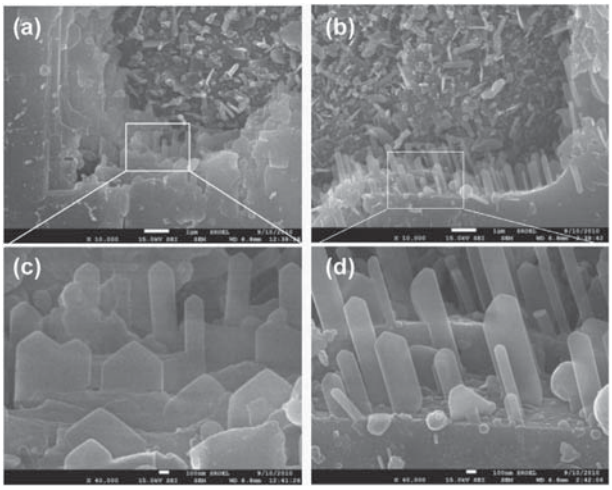

Fig. 8 (a), (b) SEM image of the region of the ablated bulk crystal. (c) and (d) are magnified sections of (a) and (b), respectively.

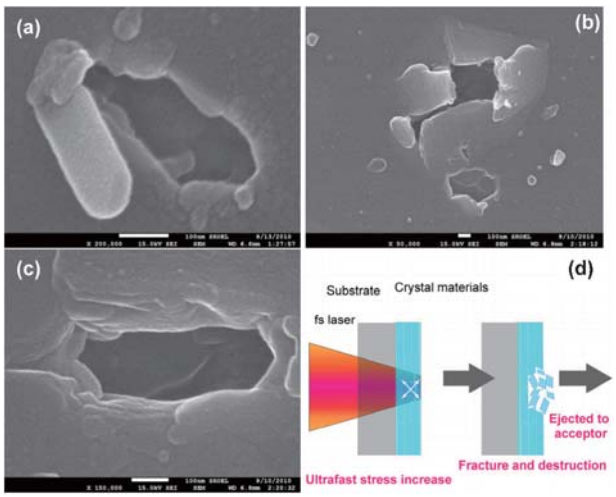

Fig. 9 (a), (b) and (c) SEM images of the region of the ablated bulk crystal 40 mJ pulse^{-1} for 10 pulses. (d) Nanoparticle formation mechanism under femtosecond laser ablation.

the laser heating takes place under nearly constant volume conditions, causing the buildup of a high thermoelastic pressure in the irradiated area.[37,38] Then, the photomechanical effects induced by the pressure relaxation start to play an important role in material ejection, as shown in Fig. 9(d). After the laser pulse duration, the significantly higher pressure will build up in the absorption region and the material ejection is driven by the relaxation of the laser-induced pressure gradient. The transient pressure induces fracture and spallation at the cleavage plane. A fraction of the ablated material was ejected in the form of particles onto the acceptor. Nanocrystals with well defined shapes might be formed from laser induced fragmentation, accompanied by a small amount of laser vapor deposition.

4. Conclusions

Femtosecond laser-induced forward transfer method has been demonstrated as an effective tool for creating organic nanocrystals. The method is simple and the size distribution of produced nanoparticles is narrow enough. The size of the prepared nanoparticles ranged from 40 to 300 nm, and the mean size could be controlled by the laser fluence. The prepared nanocrystals show well-facet shape. We believe that the present Fs-LIFT method will be applied to diverse organic compounds.

Acknowledgements

This work was supported by the Natural Science Foundation of China (NSFC) under Grant #90923037, 61127010, 61107024, and Graduate Interdisciplinary Fund of Jilin University (No. 2011J008).

References

1 Y. Chujo and T. O. Otsuka, *Polym. J.*, 2011, **43**, 352–357.
2 H. B. Fu, B. H. Loo, D. B. Xiao, R. M. Xie, X. H. Ji, H. N. Yao, B. W. Zhang and L. Q. Zhang, *Angew. Chem., Int. Ed.*, 2002, **41**, 962–965.
3 Q. Jiang, H. X. Shi and M. Zhao, *J. Chem. Phys.*, 1999, **111**, 2176–2180.
4 Z. Wen, M. Zhao and Q. Jiang, *J. Phys. Chem. B*, 2002, **106**, 4266–4268.
5 Y. S. Zhao, H. B. Fu, A. D. Peng, Y. Ma, D. B. Xiao and J. N. Yao, *Adv. Mater.*, 2008, **20**, 2859–2876.
6 S. Kim, Q. Zheng, G. S. He, D. J. Bharali, H. E. Pudavar, A. Baev and P. N. Prasad, *Adv. Funct. Mater.*, 2006, **16**, 2317–2323.
7 A. D. Peng, D. B. Xiao, Y. Ma, W. S. Yang and J. N. Yao, *Adv. Mater.*, 2005, **17**, 2070–2073.
8 Z. Y. Tian, W. W. Wu and A. D. Q. Li, *ChemPhysChem*, 2009, **10**, 2577–2591.
9 E. Botzung-Appert, V. Monnier, T. H. Duong, R. Pansu and A. Ibanez, *Chem. Mater.*, 2004, **16**, 1609–1611.
10 S. Y. Park, B. K. An, S. K. Kwon and S. D. Jung, *J. Am. Chem. Soc.*, 2002, **124**, 14410–14415.
11 H. H. Fang, Q. D. Chen, J. Yang, H. Xia, B. R. Gao, J. Feng, Y. G. Ma and H. B. Sun, *J. Phys. Chem. C*, 2010, **114**, 11958–11961.
12 H. H. Fang, B. Xu, Q. D. Chen, R. Ding, F. P. Chen, J. Yang, R. Wang, W. J. Tian, J. Feng, H. Y. Wang and H. B. Sun, *IEEE J. Quantum Electron.*, 2010, **46**, 1775–1781.
13 F. Wang, M. Y. Han, K. Y. Mya, Y. B. Wang and Y. H. Lai, *J. Am. Chem. Soc.*, 2005, **127**, 10350–10355.
14 Z. Y. Tian, Y. Chen, W. S. Yang, J. N. Yao, L. Y. Zhu and Z. G. Shuai, *Angew. Chem., Int. Ed.*, 2004, **43**, 4060–4063.
15 J. N. Yao, D. B. Xiao, X. Lu, W. S. Yang, H. B. Fu, Z. G. Shuai and Y. Fang, *J. Am. Chem. Soc.*, 2003, **125**, 6740–6745.
16 D. B. Xiao, W. S. Yang, J. N. Yao, X. Lu, Y. Xia and Z. G. Shuai, *J. Am. Chem. Soc.*, 2004, **126**, 15439–15444.
17 T. P. Radhakrishnan, A. Patra, N. Venkatram and D. N. Rao, *J. Phys. Chem. C*, 2008, **112**, 16269–16274.
18 M. Y. Han, F. Wang, K. Y. Mya, Y. B. Wang and Y. H. Lai, *J. Am. Chem. Soc.*, 2005, **127**, 10350–10355.
19 T. R. Radhakrishnan, A. Patra, N. Hebalkar, B. Sreedhar, M. Sarkar and A. Samanta, *Small*, 2006, **2**, 650–659.
20 H. Xu, S. M. Yang, D. Lu, L. L. Tian, F. He, G. Chen, F. Z. Shen and Y. G. Ma, *Nanoscale*, 2011, **3**, 2261–2267.
21 J. N. Yao and H. B. Fu, *J. Am. Chem. Soc.*, 2001, **123**, 1434–1439.
22 P. F. Barbara, J. K. Grey, D. Y. Kim, B. C. Norris and W. L. Miller, *J. Phys. Chem. B*, 2006, **110**, 25568–25572.
23 H. Kasai, H. S. Nalwa, H. Oikawa, S. Okada, H. Matsuda, N. Minami, A. Kakuta, K. Ono, A. Mukoh and H. Nakanishi, *Jpn. J. Appl. Phys.*, 1992, **31**, L1132.
24 Y. Morita, N. Nagaya, Y. Shibata, E. Kwon, H. Oikawa, H. Nakanishi, M. Kira and K. Sakamoto, *Chem. Commun.*, 2011, **47**, 2315–2317.
25 K. Baba, H. Kasai, S. Okada, H. Oikawa and H. Nakanishi, *Jpn. J. Appl. Phys.*, 2000, **39**, L1256–L1258.
26 T. Asahi, T. Sugiyama and H. Masuhara, *Acc. Chem. Res.*, 2008, **41**, 1790–1798.
27 T. Asahi, H. G. Jeon, T. Sugiyama and H. Masuhara, *Jpn. J. Appl. Phys.*, 2007, **46**, L733–L735.
28 T. Asahi, Y. Tamaki and H. Masuhara, *J. Phys. Chem. A*, 2002, **106**, 2135–2139.
29 H. W. Liu, F. Chen, X. H. Wang, Q. Yang, H. Bian, J. H. Si and X. Hou, *Thin Solid Films*, 2010, **518**, 5188–5194.
30 S. Kostler, A. Rudorfer, A. Haase, V. Satzinger, G. Jakopic and V. Ribitsch, *Adv. Mater.*, 2009, **21**, 2505–2510.
31 M. Sanz, M. Walczak, M. Oujja, C. Domingo, A. Klini, E. L. Papadopoulou, C. Fotakis and M. Castillejo, *Thin Solid Films*, 2010, **518**, 5525–5529.
32 D. P. Banks, K. S. Kaur and R. W. Eason, *Appl. Surf. Sci.*, 2009, **255**, 8343–8351.
33 D. P. Banks, C. Grivas, J. D. Mills, R. W. Eason and I. Zergioti, *Appl. Phys. Lett.*, 2006, **89**, 193107.
34 B. Tan, K. Venkatakrishnan and K. G. Tok, *Appl. Surf. Sci.*, 2003, **207**, 365–371.
35 J. Yang, H. H. Fang, R. Ding, S. Y. Lu, Y. L. Zhang, Q. D. Chen and H. B. Sun, *J. Phys. Chem. C*, 2011, **115**, 9171–9175.
36 H. Nakanotani and C. Adachi, *Appl. Phys. Lett.*, 2010, **96**, 053301.
37 L. V. Zhigilei and B. Garrison, *Appl. Surf. Sci.*, 1998, **127**, 142–150.
38 Y. Hosokawa, T. Mito, T. Tada, T. Asahi and H. M. Masuhara, *Proc. SPIE–Int. Soc. Opt. Eng.*, 2002, **4426**, 113.